(³He, n) Reaction at 25 MeV * †

M. B. Greenfield‡ and C. R. Bingham

The University of Tennessee, Knoxville, Tennessee 37916

and

E. Newman and M. J. Saltmarsh

Oak Ridge National Laboratory, Oak Ridge, Tennessee 37830

(Received 5 June 1972)

The (³He,n) reaction has been studied on targets of ^{12}C, ^{27}Al, ^{28}Si, and $^{58, 60, 62}$Ni at an incident energy of 25 MeV. The observed resolution of the neutron time-of-flight spectrometer used in this work was about 1%. Differential cross sections were obtained for the resolvable final states over the angular range of 0–40° (L). The angular distributions were compared with the predictions of a simple, one-step, two-nucleon-transfer model. In this formalism the diproton stripped from ³He is transferred to the target retaining its $^1S_0$ relative motion. The shapes of the angular distributions were unique for a given l transfer and were, in most cases, generally reproduced by the calculations. For 0^+ targets the J^π of many final states could be assigned. Comparison of experimental with theoretical relative magnitudes permitted assignment of dominant shell-model configurations. To first approximation the relative transition strengths to final states in ^{14}O, ^{30}S, and ^{60}Zn were consistent with the assumption of two particles coupled to an effectively "closed core."

1. INTRODUCTION

Advances in the understanding of the two-nucleon-transfer (2NT) reaction have made possible rather successful treatment of much of the existing data.[1-6] The 2NT stripping reactions are of particular interest for the investigation of two-particle excitations and may represent a unique method for the study of nuclei which are two nucleons removed from a stable target. When the targets investigated have some degree of shell closure and the states excited in the residual nuclei have large target ground-state parentage, 2NT stripping reactions can become powerful spectroscopic tools.

One model for the (³He, n) reaction assumes the transfer of a $^1S_0$ diproton to the target,[7] producing final states which retain the target as a core and two valence protons having singlet relative motion. One-step stripping of a singlet diproton on spin-zero targets leads to final states whose spin-parity must obey the selection rules $\Delta J = \Delta L$ and $\Delta \pi = (-1)^{\Delta L}$. Thus if the shapes of experimental angular distributions are characteristic of a particular angular momentum transfer, then a unique J^π value may be assigned.

The direct-reaction theory based on the above model has been quite successful in reproducing the observed features of recent two-neutron-transfer data.[1-4] Two-proton-transfer data have been somewhat more difficult to obtain. The (³He, n) reaction is difficult experimentally, while for the alternative heavy-ion-induced reactions the observed angular distributions are both struc-

tureless and quite similar from level to level.[8] In addition the simplifying assumption of a $^1S_0$ diproton transfer is not necessarily valid in heavy-ion reactions.

Previous (³He, n) studies have been made either at incident energies of less than 15 MeV or with energy resolution insufficient to permit separation of the final states.[9-16] A study of the reaction at relatively high incident energy has the advantage of enhancing the direct reaction, minimizing compound-nuclear effects, and providing for a more reliable application of distorted-wave theory.[17] The failure of direct-reaction theory to account for many of the observed features of existing (³He, n) data may be due to misapplication of the distorted-wave theory at low incident energy or to a misinterpretation of the reaction mechanism. The 25-MeV incident energy used in this (³He, n) study represents a compromise between the advantages of higher energy and the need for sufficient energy resolution in the neutron time-of-flight spectrometer.

2. EXPERIMENTAL METHOD

The neutron time-of-flight spectrometer and scattering chamber described below were designed using the parameters associated with the singly charged 25-MeV ³He beam from the Oak Ridge isochronous cyclotron (ORIC) as a starting point. This same system has recently been used successfully to study the (p, n) reaction at 30 MeV.[18]

The high-intensity (~10-μA) ³He beam has an energy spread [full width at half maximum (FWHM)] of less than 100 keV and a microburst width of ~2.5 nsec. The cyclotron repetition period was 116 nsec. Target thicknesses were selected so that the beam energy losses were less than 100 keV. The detector was a 15-cm-diam by 10-cm-thick cylindrical cell of NE-213 coupled to XP-1040 photomultiplier. The time jitter of the cell plus photomultiplier was measured to be less than 1 nsec. With these experimental conditions a 35-m flight path was required to obtain an over-all energy resolution of about 1% for 10–35-MeV neutrons.

The physical layout is shown schematically in Fig. 1. The ³He beam was deflected by a switching magnet, which was used as the target chamber. Faraday cups were provided for both left and right deflections and were placed so that radiation from them could not be seen by the detector. Neutrons from the target passed through a plastic vacuum flange, 16 m across the experimental room, through a hole in the 2-m concrete shield wall, and 17 m more to the neutron detector. A defining collimator with a 2.0-cm-diam hole centered on the flight path was positioned about 1.5 m from the target. A clearing collimator with a 10×10-cm slot was located directly in front of the shield wall. Only neutrons originating from the target and not those from collimators, target frames, etc., could reach the detector.

The constraint that the flight path pass through a fixed hole in the shield wall made it necessary to use the beam switching magnet for scattering angle variations. The effective scattering angle was varied by changing the angle at which the beam strikes the target. This was accomplished by positioning the target at various points on the beam trajectories (see Fig. 1). The laboratory scattering angle was calculated from the position of the target and the beam trajectory in the magnet. The absolute error in the scattering angle was less than 0.2°. Collimators were repositioned for each angle, and the flight path was a function of the target position.

The heavy shielding satisfactorily removed the cyclotron-dependent background. In order to reduce the prompt γ flash, as well as cyclotron-independent (time-uncorrelated) sources of background, neutron-γ pulse-shape discrimination techniques were employed.[19] Background from cosmic radiation was further reduced by an anti-coincidence detector. Figure 2 shows an example of the separation between neutrons and γ rays above a threshold of about one light unit.

Data were recorded as time of flight vs pulse height in a 400 ×50 multichannel analyzer. γ events were stored in the first Y plane, and the remaining 49 plane were used for the neutron spectra. The content of the analyzer memory was transferred to an on-line computer for data reduction and spectrum stripping. Since the pulse height of each neutron event was recorded, the effective neutron threshold could be selected during analysis. The threshold was calibrated relative to the ²²Na 1.28-MeV γ ray. The detection efficiency was determined from a Monte Carlo calculation.[20] The error associated with the ab-
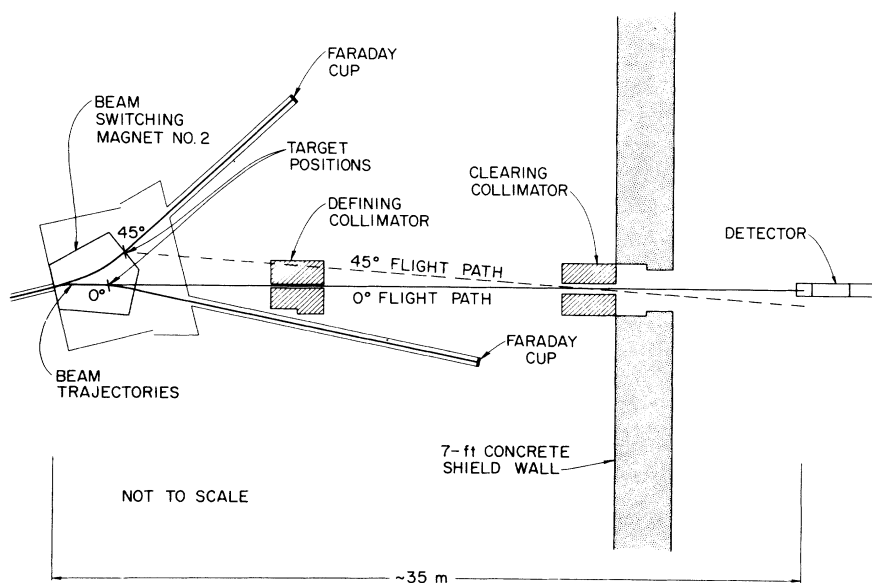

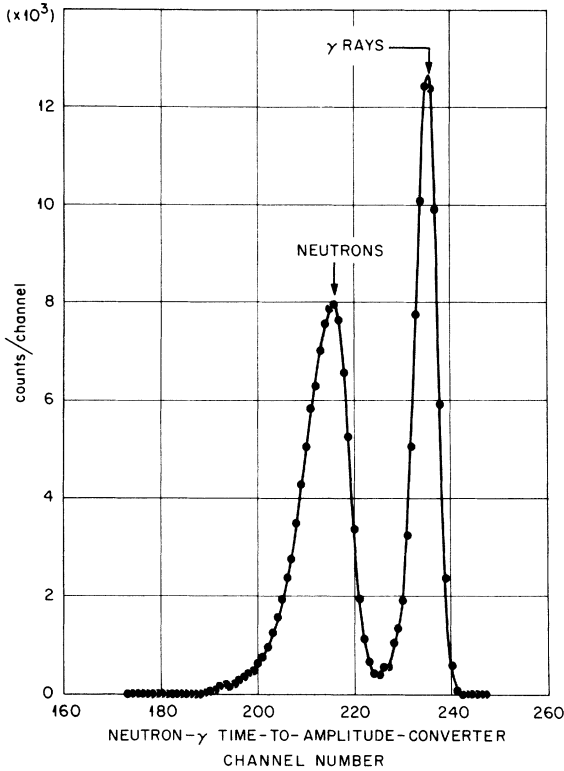FIG. 1. Schematic layout of the ORIC neutron time-of-flight line.

FIG. 2. Neutron-γ separation from the pulse-shape discrimination for the ^{12}C$(^3$He$,n)^{14}$O reaction at an incident energy of 25.4 MeV.

solute efficiency is estimated to be less than 20%, whereas the relative uncertainty is less than 5%.

The time axis of each spectrum was derived from a time calibration spectrum, consisting of peaks separated by 25 nsec. A time calibration signal, electronically processed in identically the same way as a true event, was introduced into the system during the dead time following each cosmic anticoincidence event. The resulting calibration produced a relative time-scale accuracy of better than ±0.03 nsec. The uncertainty in the total time of flight was, for the most part, given by the statistical uncertainty in defining neutron peak centroids and was typically between 0.1 and 0.3 nsec. An external beam sweeper was used to suppress two out of three beam bursts, thus sufficiently increasing the period so that time overlap was not a problem for the neutron energies observed.

The differential cross sections to most low-lying final states of the residual nuclei studied were obtained with little difficulty. For some of the final nuclei some states at high excitation were not completely resolved. Yields for these peaks were determined by means of a Gaussian peak-fitting routine. In general, background was sufficiently reduced so that cross sections on the order of 50 μb/sr could be measured. The differential cross sections were corrected for the neutron attentuation along the 35-m flight path.

TABLE I. Global optical parameters.

Parameter set	V (MeV)	W (MeV)	r_0 (fm)	r_i (fm)	r_c (fm)	a_0 (fm)	a_i (fm)	W_0 (MeV)
			Incident channel					
I	170.0	20.0	1.14	1.82	1.40	0.67	0.56	$\cdots$
II	146	18.4	1.40	1.40	1.25	0.55	0.55	$\cdots$
III	198	20.0	1.50	1.50	1.25	0.55	0.55	$\cdots$
IV [a]	146.5	$\cdots$	1.25	1.25	1.25	0.65	0.47	36.5
V [a]	220.0	12.4	1.16	1.55	1.3	0.597	1.046	
^{58}Ni VI [b]	172.6	20.16	1.147	1.562	1.25	0.712	0.802	$\cdots$
^{62}Ni VII [c]	174.9	22.74	1.14	1.522	1.25	0.747	0.782	$\cdots$
VIII [c]	174.5	22.64	1.14	1.525	1.25	0.747	0.787	19.0
			Exit channel					
I [d]	$F(E)$	5.75	1.25	1.25	$\cdots$	0.65	0.70	$\cdots$
II [e]	$F(E)$	$F(E)$	$F(A)$	$F(A)$	$\cdots$	0.66	0.48	$\cdots$
III [f]	$F(E, (N-Z)/A)$	$F(A)$	1.25	1.25	$\cdots$	0.65	0.47	$\cdots$
IV [g]	$F(E, (N-Z)/A)$	$F(E)$	1.17	1.26	$\cdots$	0.75	0.58	$\cdots$

[a] Reference 26.
[b] Reference 27.
[c] Reference 28.
[d] Reference 29.

[e] Reference 30.
[f] Reference 31.
[g] Reference 32.

TABLE II. Q values.

Reaction	Q value This work (MeV)	Q value Previous work (MeV)
^{27}Al(^{3}He, n)^{29}P	6.616 ± 0.03	6.609 ± 0.006
^{58}Ni(^{3}He, n)^{60}Zn	0.821 ± 0.013	0.818 ± 0.018
^{60}Ni(^{3}He, n)^{62}Zn	3.580 ± 0.03	3.512 ± 0.014
^{62}Ni(^{3}He, n)^{64}Zn	6.118 ± 0.012	6.112 ± 0.007

Both the relative errors in energy determinations and differential cross sections were determined essentially by counting statistics. Absolute uncertainties in the differential cross sections were dominated by uncertainties in the absolute detection efficiency and the neutron attentuation in the flight path and were in general less than ±25%.

3. THEORY

The data obtained in this study were compared with calculations of the zero-range 2NT option of JULIE.[21] Recent calculations of finite-range ef-

fects by Bayman[22] and Rost and Kunz[23] indicate that the zero-range approximation is valid for 2NT from a mass-three projectile. That is, the finite-range and zero-range predictions agree except in absolute magnitude. The finite-range predictions of Bayman predict magnitudes about one third of those observed, whereas the zero-range calculations of the JULIE code are not absolute. In this work calculated transition strengths were normalized to the ground-state transition.

In general 2NT cross sections are calculated from a coherent summation of transition amplitudes from pairs of particles which couple to the same resultant final-state quantum numbers. The two-nucleon JULIE code calculates complex transition amplitudes, $A(j_1 j_2 J_f \theta)$, for the transfer of a pair of particles $n_1 l_1 j_1; n_2 l_2 j_2$ coupled to resultant angular momentum J_f. Included in this amplitude are: (1) the kinematic amplitude which is identical in form to the single-nucleon-transfer kinematic amplitude,[24-25] (2) the overlap of the relative motion of the diproton in the bound state with its initial motion in the incident projectile, (3) a Moshinsky bracket transforming from the original
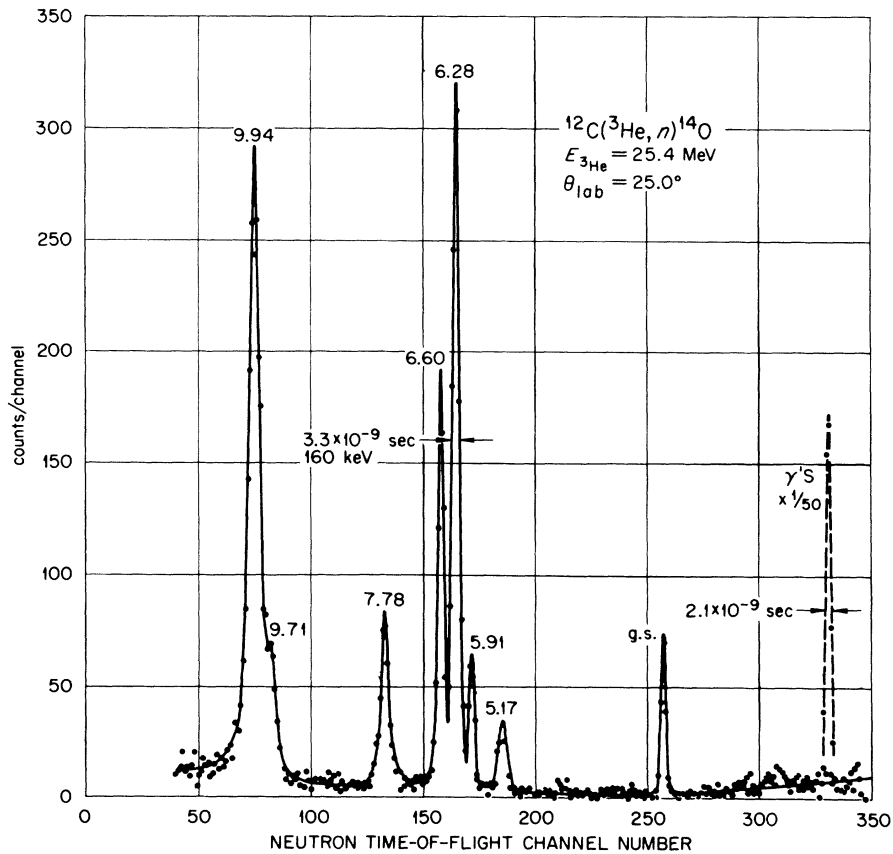

FIG. 3. Neutron time-of-flight spectrum from the ^{12}C(^{3}He,n)^{14}O reaction at 25.4 MeV. The prompt γ flash has been superimposed on the spectrum.

TABLE III. Excitation energies and J^π values for levels observed in the $(^3\text{He}, n)$ reaction together with previously published results.

Residual nucleus	Present work		Previous work	
	Excitation energy (MeV)	J^π	Excitation energy (MeV)	J^π
^{14}O	0.00	0^+	0.00	0^+
	5.173 ± 0.010	1^-	5.17 ± 0.04	(1^-)
	5.930 ± 0.015	0^+	5.91 ± 0.04	(0^+)
	6.272 ± 0.010	3^-	6.28 ± 0.03	(3^-)
	6.596 ± 0.010	(2^+)	6.60 ± 0.03	2^+
	$\cdots$		6.79 ± 0.03	(2^-)
	7.768 ± 0.010	2^+	7.78 ± 0.03	2^+
	$\cdots$		8.74 ± 0.060	
	9.705 ± 0.025	(2^+)	9.74 ± 0.030	
	9.915 ± 0.020	4^+		
^{29}P	0.00	$\cdots$	0.00	$1/2^+$
	1.32 ± 0.06	$\cdots$	1.38	$3/2^+$
	1.97 ± 0.02	$\cdots$	1.96	$5/2^+$
	$\cdots$	$\cdots$	2.40	$\cdots$
	3.33 ± 0.04	$\cdots$	$\begin{cases} 3.10 \\ 3.47 \end{cases}$	$5/2^+$; $\cdots$
	4.24 ± 0.06	$\cdots$	$\begin{cases} 4.08 \\ 4.34 \end{cases}$	$\cdots$; $3/2^-$
	4.88 ± 0.06	$\cdots$	$\begin{cases} 4.77 \\ 4.97 \end{cases}$	$1/2^+$; $\cdots$
	5.66 ± 0.07	$\cdots$	$\begin{cases} 5.30 \\ 5.53 \\ 5.74 \end{cases}$	$\cdots$; $1/2^-$; $5/2^-$
	$\cdots$	$\cdots$	5.97	$3/2^+$
	$\cdots$	$\cdots$	6.20	$3/2^-$
	6.52 ± 0.06	$\cdots$	$\begin{cases} 6.33 \\ 6.54 \\ 6.59 \end{cases}$	$\cdots$; $\cdots$; $1/2^+$
			$\vdots$	
	8.32 ± 0.09	$\cdots$	$\begin{cases} 8.20 \\ 8.26 \\ 8.36 \end{cases}$	$\cdots$; $\cdots$; $\cdots$
	10.13 ± 0.10		$\cdots$	$\cdots$
	11.16 ± 0.10		$\cdots$	$\cdots$
	11.80 ± 0.10		$\cdots$	$\cdots$
^{30}S	0.00	0^+	0.00	(0^+)
	2.22 ± 0.025	(2^+)	2.210 ± 0.03	(2^+)
	3.41 ± 0.030	(0^+)	3.43 ± 0.03	$\cdots$
	3.69 ± 0.030	(2^+)	3.71 ± 0.03	$\cdots$
	5.21 ± 0.050	(3^-)	$\cdots$	$\cdots$
	6.11 ± 0.050	(5^-)	$\cdots$	$\cdots$
^{60}Zn	0.00	(0^+)	0.00	(0^+)
	1.019 ± 0.010	2^+	1.019 ± 0.025	$\cdots$
	2.21 ± 0.03	(4^+)	$\cdots$	$\cdots$
	3.51 ± 0.02	0^+	$\cdots$	$\cdots$
	4.18 ± 0.03	$(0^+, 2^+)$	$\cdots$	$\cdots$
	4.93 ± 0.04	(2^+)	$\cdots$	$\cdots$
	5.49 ± 0.03	(4^+)	$\cdots$	$\cdots$
^{62}Zn	0.00	(0^+)	0.00	$\cdots$
	0.964 ± 0.010	2^+	$\cdots$	$\cdots$
	3.17 ± 0.03	$\cdots$	$\cdots$	$\cdots$
	3.87 ± 0.03	$\cdots$	$\cdots$	$\cdots$
	5.34 ± 0.03	$\cdots$	$\cdots$	$\cdots$
	5.70 ± 0.03	$\cdots$	$\cdots$	$\cdots$

TABLE III *(Continued)*

Residual nucleus	Present work Excitation energy (MeV)	J^π	Previous work Excitation energy (MeV)	J^π
^{64}Zn	0.00	(0^+)	0.00	0^+
	1.024 ± 0.02	2^+	0.992	2^+
	$\cdots$	$\cdots$	1.80	2^+
	$\cdots$	$\cdots$	1.91	(0^+)
	$\cdots$	$\cdots$	2.29	(4^+)
	$\cdots$	$\cdots$	2.35	$\cdots$
	$\cdots$	$\cdots$	2.59	(0^+)
	$\cdots$	$\cdots$	2.73	$\cdots$
	2.93 ± 0.05	$\cdots$	2.99	(3^-)
			$\vdots$	
	3.70 ± 0.07	$\cdots$	3.84	$\cdots$
	4.20 ± 0.08	$\cdots$	$\begin{cases} 4.12 \\ 4.22 \\ 4.49 \end{cases}$	$\cdots$
	$\cdots$	$\cdots$	4.66	$\cdots$
	5.20 ± 0.10	$\cdots$	5.2	$\cdots$

single-particle coordinates of the transferred pair to singlet relative and center-of-mass coordinates, (4) an LS-jj recoupling coefficient, and (5) appropriate Clebsch-Gordan coefficients.

The distorted waves (which enter in term 1) were calculated from the optical-model parameters[26]-[32] shown in Table I. These parameters are the results of searches designed to fit elastic scattering data for a wide range of energies and targets. Other ^{3}He optical parameters derived from the appropriate elastic scattering were used when available.

Two-particle final-state wave functions describing the center-of-mass motion of the diproton with respect to the core were generated from a Woods-Saxon well with the well depth adjusted such that the particle separation energy was an eigenvalue. Geometric parameters for the bound-state well were chosen as $r_0 = 1.15$ fm, $r_c = 1.15$ fm, and $a_0 = 0.45$–0.65 fm. The shapes of the calculated angular distributions were generally insensitive to these parameters. The resultant final-state wave functions were expanded in a finite series of harmonic-oscillator functions so that the overlap involved in terms (2) and (3) above might be obtained in a closed form.[33]

In order to obtain differential cross sections from the transition amplitudes $A(j_1 j_1 J_f \theta)$, one must determine the extent to which the final state looks like the core plus two nucleons in the single-particle state $n_1 l_1 j_1$; $n_2 l_2 j_2$ coupled to J_f. If $B(j_1 j_2 J_f)$ are the two-nucleon spectroscopic amplitudes as defined by Yoshida,[34] then the relative

cross sections are given by

$$\sigma_J(\theta) \propto \frac{(2J_f + 1)}{(2J_i + 1)} \left| \sum_{j_1 j_2} B(j_1 j_2 J_f) A(j_1 j_2 J_f \theta) \right|^2,$$

where $\vec{j}_1 + \vec{j}_2 = \vec{J}_f$. It is important to note here that the spectroscopic amplitudes enter in a coherent summation. Unless the final state is defined by a single, pure two-particle configuration, it is not possible to determine spectroscopic amplitudes uniquely from experimentally determined cross sections. For this reason the calculations in this work were primarily used: (1) to determine dominant two-particle configurations in the final-state wave functions or (2) as a check on existing model wave functions. Parameters chosen for a particular calculation are designated for example as I-C-II, indicating ^{3}He parameter Set I, shell-model wave functions C, and neutron parameters II.

4. EXPERIMENTAL RESULTS AND COMPARISON WITH THEORY

Neutron time-of-flight spectra were obtained for the (^{3}He, n) reactions leading to final states of ^{14}O, ^{29}P, ^{30}S, ^{60}Zn, ^{62}Zn, and ^{64}Zn. Excitation energies were determined from the time calibration discussed in Sec. 2 and used the ^{12}C(^{3}He, n)^{14}O Q value as absolute reference. To minimize error due to beam energy fluctuations and electronic drift Q values for the reactions studied were determined by alternatively accumulating data on

^{12}C and the target in question with cy ₃ times of 2–10 min. In Table II we compare the Q values determined here with those established in previous work.[13, 14, 35] The agreement is quite satisfactory except for ^{60}Ni where the discrepancy is quite large. This seems not to be the result of a systematic error, since both more positive and more negative values are in agreement with previous work.

The shapes of experimental angular distributions were generally characteristic of the angular momentum transfer, but were insensitive to the final-state two-particle structure. Calculations are shown normalized to the data for the purpose of extracting spins and parities. The calculated mag-

FIG. 4. Angular distributions of neutrons from the ^{12}C-(^{3}He,n)^{14}O reaction. Solid curves are the results of two-nucleon-transfer distorted-wave calculations assuming the final-state configurations shown with each curve in the figure. The dashed curves show the effect of modifying the exit-channel imaginary radius to account for the different matter distributions for the various final states.

nitudes were quite sensitive to the assumed structure of the final states. From a comparison of the predicted and observed magnitudes, estimates of the dominant two-particle structure of the final nuclei could be obtained.

$^{12}C(^3He,n)^{14}O$. A neutron time-of-flight spectrum from the ^{12}C(^{3}He, n)^{14}O reaction is shown in Fig. 3. The prompt γ flash, as well as a time-independent background of about 100 counts/channel were removed from the data by the neutron-γ discrimination system. The prompt γ flash, shown as the dashed peak with a time width of 2.1 nsec FWHM, was used as an absolute time calibration. The over-all energy resolution for detection of 16-MeV neutrons is 160 keV (FWHM). Table III shows the excitation energies of the neutron groups observed and previously reported values. The Q value was not experimentally determined for this reaction, but was used as a calibration. The previously reported (2^-) level at 6.79 MeV[36] was not observed here in agreement with the selection rules.

Angular distributions of neutrons from all the observed levels were obtained from 0 to 35° lab. The uncertainty in the background subtraction from peak areas was negligible. The levels near 6 and 10 MeV excitation were not completely resolved. For these a peak-fitting program assuming Gaussian peak shapes was used to extract the areas. Figure 4 shows the angular distributions of neutrons for all the observed levels. Error bars indicate the total relative errors and largely reflect statistical error. The uncertainty in the absolute normalization is about 22%.

Distorted-wave calculations were attempted with several combinations of the optical parameter sets from Table I. Although the shapes of angular distributions were not extremely sensitive to the particular sets chosen, those which gave the most consistent fits to the levels observed were ^{3}He Sets III and V and neutron Set III. The final-state wave functions were constructed by the previously mentioned method with the pure two-particle shell configurations shown with each curve in Fig. 4. The shapes of calculated angular distributions were characteristic of a particular angular momentum transfer, but were generally insensitive to a 15% variation of the bound-state geometric parameters. All the levels in ^{14}O except the ground state are either unbound or only slightly bound. In analogy with the earlier single-nucleon work we chose to perform these calculations by assuming the levels to be bound and then extrapolating the effects on the shape and magnitude into the unbound region. For the single-nucleon case this method has been compared with more rigorous calculations[37-39] and the agreement is on the order of[40] 15%. For the appropriate states in ^{14}O it was
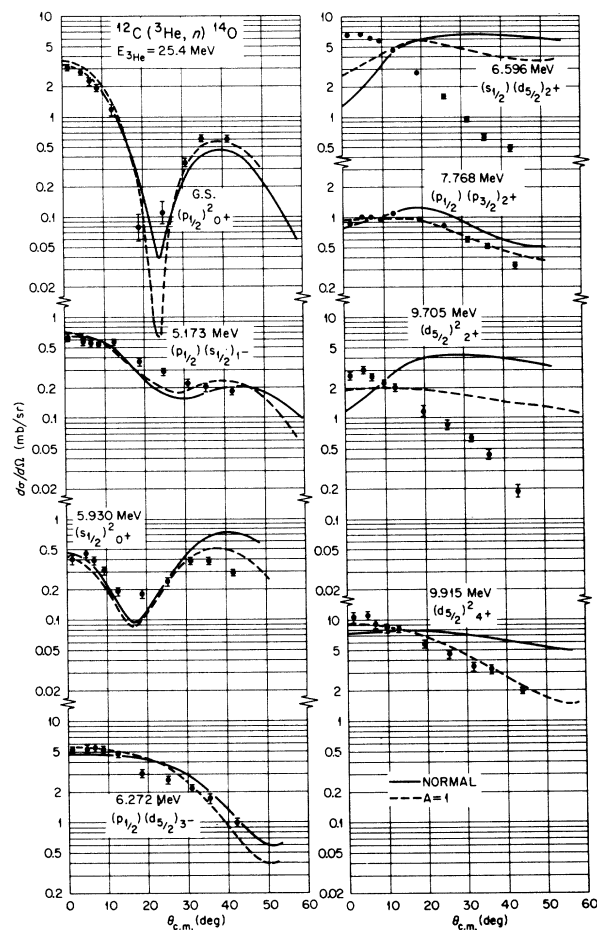
TABLE IV. Comparison of the observed and calculated relative magnitudes to levels in ^{14}O from the ^{12}C(^{3}He, n)^{14}O reaction.

^{14}O excitation	J^π	R_{exp}	V-T-III	III-T-III	V-M-III	III-M-III	Dominant two-particle structure
g.s.	0^+	1.0	1.0	1.0	1.0	1.0	$(p_{1/2})^2$
5.173	1^-	0.2	1.2	3.0	1.2	1.9	$(p_{1/2})(s_{1/2})$
5.930	0^+	0.2	2.8	1.2	1.8	1.0	$(s_{1/2})^2$
6.272	3^-	1.7	2.5	2.1	1.9	1.1	$(p_{1/2})(d_{5/2})$
6.596	2^+	2.1	1.8	2.9	1.2	2.4	$(s_{1/2})(d_{5/2})$ $(d_{5/2})^2$ $(s_{1/2})(d_{3/2})$
7.768	2^+	0.3	0.7	1.8	0.5	0.6	$(s_{1/2})(d_{5/2})$ $(d_{5/2})^2$ $(s_{1/2})(d_{3/2})$
9.705	2^+	0.9	0.7	3.2	$\cdots$	$\cdots$	$(s_{1/2})(d_{3/2})$ $(d_{5/2})^2$
9.915	4^+	3.3	1.6	4.0	$\cdots$	$\cdots$	$(d_{5/2})^2$

found that the shapes of the angular distributions remained nearly constant as a function of separation energy, whereas the magnitudes did not. The solid curves shown with the data in Fig. 4 were obtained by exponentially extrapolating the bound-state calculations into the unbound region.

The shapes of the angular distributions are characteristic of a particular angular momentum transfer and lead to definite J^π assignments with the exception of the 2^+ levels at 6.596 and 9.705 MeV. A definite 2^+ assignment for the 6.596 and 7.768 levels has been established in the ^{14}N(^{3}He, t)^{14}O reaction.[37] However, in a recent study of the ^{16}O-

(p, t)^{14}O reaction with polarized protons the 6.596-MeV level was reported to exhibit an "anomalous behavior."[41] Possible explanations applicable here are that a more realistic interaction potential with finite range is needed or that a more complex reaction mechanism is responsible. If those incon-
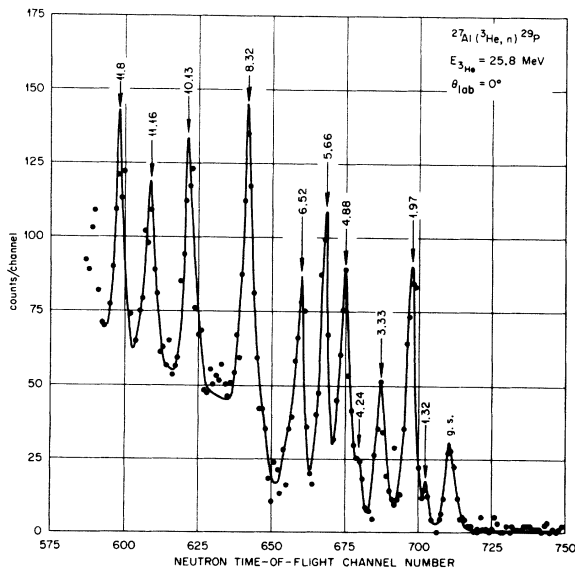

FIG. 5. Neutron time-of-flight spectrum from the ^{27}Al-(^{3}He,n)^{29}P reaction. The peaks are labeled with the excitation energies measured in this study.
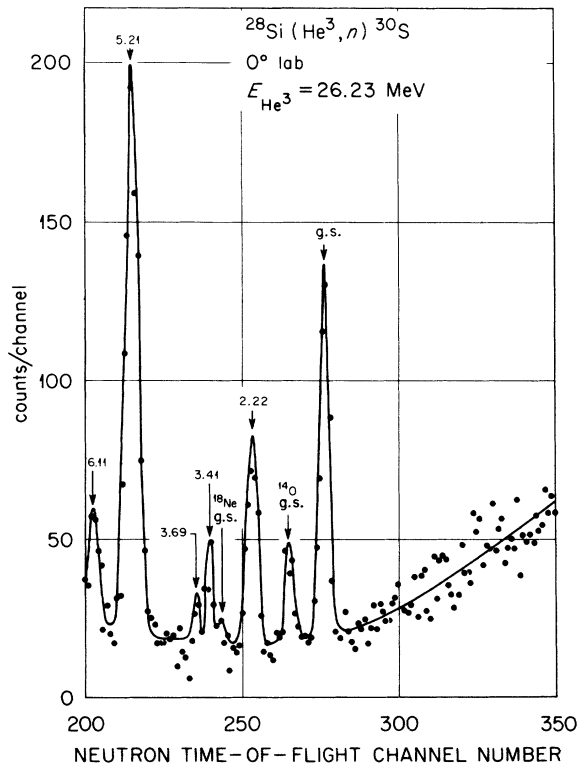

FIG. 6. Neutron time-of-flight spectrum from the ^{28}Si-(^{3}He,n)^{30}S reaction. Peaks are labeled with the excitation energies measured in this study.

sistencies are due to a general misunderstanding of the reaction mechanism, then the present theory should not be so successful in predicting the observed structure of the other angular distributions. The best evidence for a competing reaction process (two-step stripping or knockout) would be the presence of non-normal-parity states which are forbidden in a one-step process by the selection rules. As noted above, the 2⁻ level is not evident in the data. Since the levels in question are unbound we may, in fact, by using faulty assumptions in the extrapolation of angular distributions into the unbound region.

An alternative explanation may be due to the treatment of the exit-channel optical parameters. One may assume that the exit-channel optical parameters should, to some degree, reflect the position of the two loosely bound transferred protons. The root-mean-squared (rms) radius of the two protons $\langle r_{2p}^2 \rangle^{1/2}$ in p-shell configurations is approximately equal to the core radius, while protons in s-d-shell configurations have nearly twice the rms radius of the core $\langle r_c^2 \rangle^{1/2}$. Such drastic changes in the surface-matter distribution are in no way accounted for in the standard optical-model analysis. In order to explore possible effects on the differential cross sections due to changes in matter distributions, a calculation with the imaginary radius adjusted by a factor $\langle r_{2p}^2 \rangle^{1/2}/\langle r_c^2 \rangle^{1/2}$ is shown as the dashed curve in Fig. 4 and is compared with a standard calculation, shown as the solid curve in Fig. 4. Intermediate values of the imaginary radius produced curves bounded by the two shown. The fits to the data with the adjusted radius are better in nearly every case. They suggest that a simple $A^{1/3}$ matter distribution is an oversimplification for light nuclei where structure in valence nucleons can have a significant effect on the over-all matter distribution. Interestingly, if the exit-channel imaginary geometry is held constant but the real diffuseness is decreased by 30%, much the same effect on the calculation is observed.

Although the shapes of the angular distributions were fairly insensitive to the final-state wave
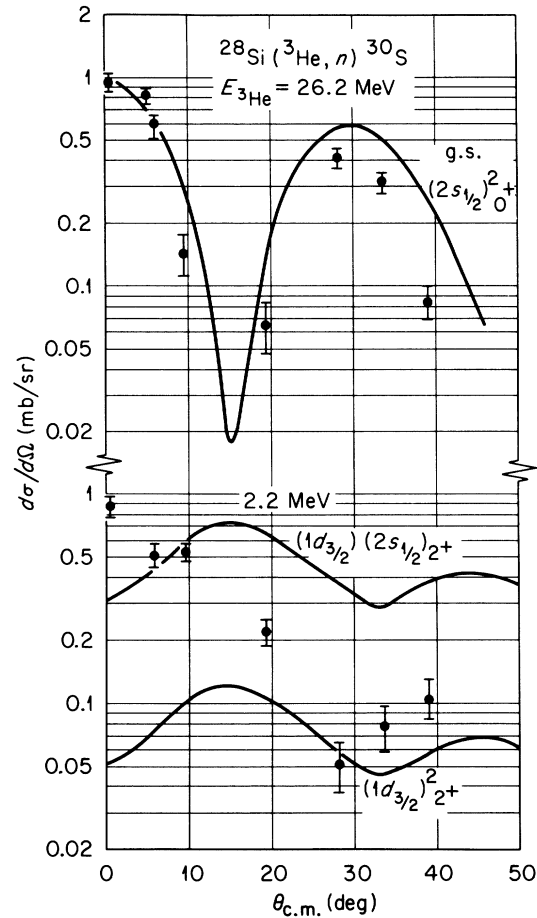

FIG. 7. Angular distribution of neutrons from the ^{28}Si(^{3}He,n)^{30}S reaction. The curves are the results of distorted-wave calculations. The two curves shown with the first excited 2^+ state indicate the magnitude relative to the ground state for the configurations shown.

functions used in the calculations, the relative magnitudes were not. The relative magnitudes of the calculated cross sections were determined for several sets of wave functions and were compared with the corresponding experimental relative magnitudes. Pure two-particle wave functions, as well as the mass-14 wave functions of True[42] (T)

TABLE V. Comparison of the experimental and calculated relative magnitudes for the ^{28}Si(^{3}He, n)^{30}S reaction.

^{30}S excitation energy (MeV)	J^π	$R_{\exp}$	R_{calc} I-B-IV	Dominant configuration B
0.00	0^+	1.0	1.0	$(2s_{1/2})^2$
2.22	(2^+)	0.50—0.90	0.46	$(2s_{1/2})(1d_{3/2})$
3.41	$(0^+),(2^+)$	0.15—0.30	0.08, 0.10	$(1d_{3/2})^2$
3.69	$(2^+),(0^+)$	0.20—0.35	0.10, 0.08	$(1d_{3/2})^2$
5.21	(3^-)	1.2 —1.9	2.20	$(1f_{7/2})(2s_{1/2})$
6.11	(5^-)	0.30—0.60	0.28	$(1f_{7/2})(1d_{3/2})$

and McGrory[43] (M) were used in the calculations. The T set was based on a ^{12}C core with active $p_{1/2}$, $s_{1/2}$, $d_{5/2}$, and $d_{3/2}$ orbitals. The M set was also based on a closed ^{12}C core with active $p_{1/2}$, $s_{1/2}$, and $d_{5/2}$ shells. Table IV shows the experimental and calculated relative magnitudes for all the observed levels for two sets of incident-channel optical parameters. The results for the pure two-particle configurations produced very poor agreement and are not shown in the table. The observed cross sections for the 1⁻ and first excited 0⁺ levels are considerably smaller than those predicted. This may, in some way, result from the assumed closed ^{12}C core. It would also appear that each of the theoretical wave functions does well for some of the states above 6.2 MeV, but miss on others. No clear cut preference for either the True or McGrory set can be drawn from this work.

$^{27}Al(^{3}He,n)^{29}P$. Figure 5 shows a neutron time-of-flight spectrum from the $^{27}Al(^{3}He, n)^{29}P$ reactions. The energies of the excited states in the figure are those found here, and the Q value was measured to be 6.616 ± 0.03 MeV. Since the spin-parity of the ground state of ^{27}Al is $\frac{5}{2}^+$, the orbital angular momentum transfer no longer uniquely defines the final state J^π. The level density becomes quite high for excitations greater than about 3 MeV, and it was not possible to resolve all of the levels above this excitation. Although the levels at about 8 MeV excitation are unstable to particle decay, it is interesting to note the strength with which these levels are populated. These levels appear as strong sharp peaks with widths of less than
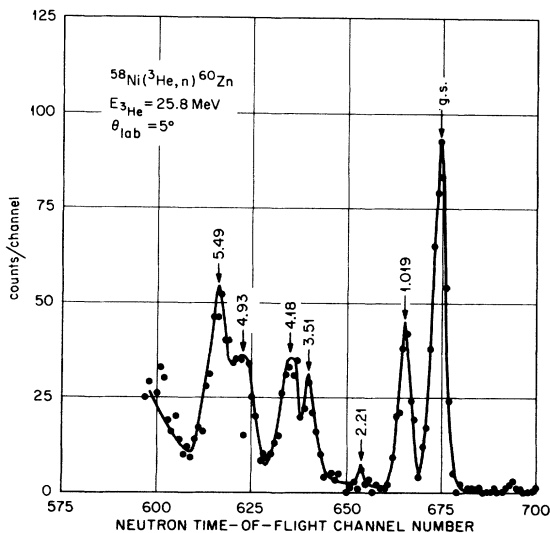
300 keV. Table III shows the ^{29}P levels observed and those previously reported.

After observing the delayed protons following the decay of ^{29}S, Hardy and Verrall[44] predicted the allowed β^+ transitions to the $T = \frac{3}{2}$ states of
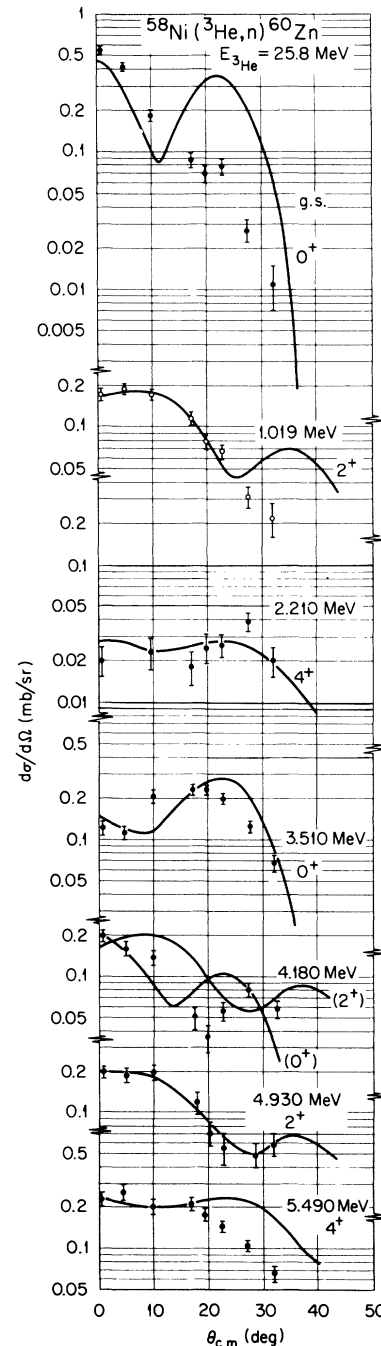

FIG. 9. Angular distributions and distorted-wave calculations for the states observed in the $^{58}Ni(^{3}He,n)^{60}Zn$ reaction.

FIG. 8. Neutron time-of-flight spectrum for the $^{58}Ni(^{3}He,n)^{60}Zn$ reaction.

TABLE VI. Comparison of the experimental and calculated relative magnitudes in the ^{58}Ni(^{3}He, n)^{60}Zn reaction.

^{60}Zn excitation	J^π	$R_{\exp}$	R_{calc} I-S-I	VI-S-I	Dominant configurations
g.s.	0^+	1.0	1.0	1.0	$(f_{5/2})^2$, $(p_{3/2})^2$, $(p_{1/2})^2$
1.019	2^+	0.63	1.07	1.11	$(p_{3/2})^2$, $(p_{3/2}, p_{1/2})$, $(p_{1/2}, f_{5/2})$, $(p_{3/2}, f_{5/2})$, $(f_{5/2})^2$
2.210	4^+	0.14	0.13	0.13	$(p_{3/2}, f_{5/2})$, $(f_{5/2})^2$
3.51	0^+	0.92	1.24	0.94	$(p_{3/2})^2$, $(p_{1/2})^2$, $(p_{5/2})^2$

^{29}P which lie at 8.08 and 8.36 MeV excitation. If one applies the semiempirical mass formula of Jaenecke,[45] the lowest $T = \frac{3}{2}$ level in ^{29}P should be at 8.2 ± 0.5 MeV. It is reasonable to assume that the strong transitions in the region of 8 MeV are the $T = \frac{3}{2}$ isobaric analogs of ^{29}S.

$^{28}Si(^3He, n)^{30}S$. Figure 6 shows a neutron time-of-flight spectrum from the ^{29}Si(^{3}He, n)^{30}S reaction at $0°$ (L). The uncertainty in the target thickness and presence of carbon and oxygen impurities prevented an accurate determination of both the reaction Q value and the absolute cross sections. Table III shows the observed levels of ^{30}S and those previously reported. The angular distributions for the ground and 2.22-MeV states are shown in Fig. 7. Distorted-wave calculations were

FIG. 10. Neutron time-of-flight spectrum for the ^{60}Ni(^{3}He, n)^{62}Zn reaction.

attempted with several choices of the optical parameters shown in Table I. The calculated shapes of the angular distributions were slightly sensitive to the particular choice of optical parameters; however, none gave consistent fits to both levels. The curves shown are the calculations with optical-model parameters I and IV in the entrance and exit channel, respectively. The curves shown are normalized to the ground-state data. The bound-state radius parameter was set at 1.15 fm with a diffuseness of 0.65 fm. The final-state nuclear wave functions were assumed to be pure two-particle configurations of $\pi(2s_{1/2})^2_{0^+}$ and $\pi(1d_{3/2}2s_{1/2})_{2^+}$ outside an inert closed $\pi(d_{5/2})^6_{0^+}\nu(d_{5/2})^6_{0^+}$ core. The shapes of the calculated angular distributions were insensitive to small adjustments in the bound-state geometric parameters, as well as the assumed two-particle ^{30}S wave functions. The poor fits to the angular distributions make it very difficult to draw any conclusions about the nuclear wave functions from the relative magnitudes at $0°$. Thus for this case we chose to obtain the relative strengths by averaging over several angles. In Table V, where the experimental and calculated relative magnitudes are compared, the spread in values reflects the differences between the zero-degree and the angle-average normalizations. It is interesting to note that the strongest transitions predicted is to the $(f_{7/2}, s_{1/2})$ 3^- configuration and the state at 5.21 MeV is consistently the most strongly excited state observed. The general consistency between the calculated and observed magnitudes gives support to the assumption that the pure two-particle configurations are the dominant components of the final-state wave functions.

$^{58, 60, 62}Ni(^3He, n)^{60, 62, 64}Zn$ reactions. Figure 8 shows a neutron time-of-flight spectrum from the ^{58}Ni(^{3}He, n)^{60}Zn (58–60) reaction. The ^{60}Zn levels observed here and those previously reported are given in Table III. The group at 4.93 may represent two or more unresolved levels. In Fig. 9 the angular distributions for six of the ^{60}Zn levels are presented. The absolute cross sections are believed to be accurate to better than 25%.

Distorted-wave calculations were attempted

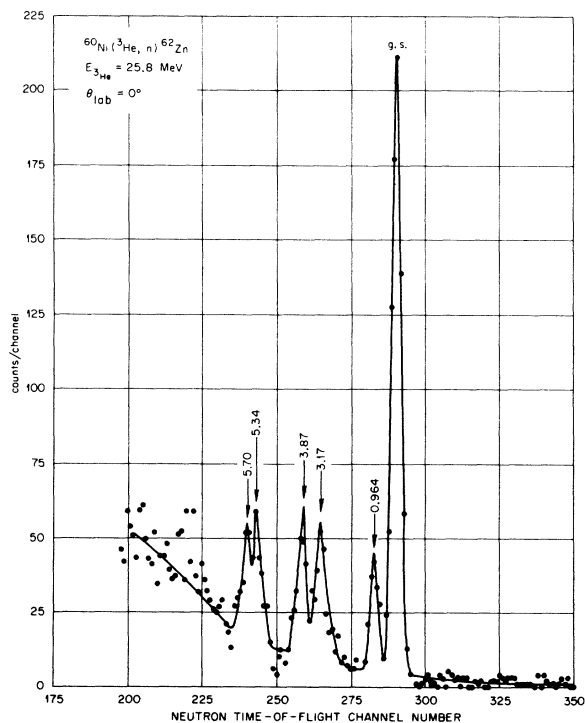with several choices of the optical parameters of Table I. The most consistent fits to all the levels observed were obtained with ^{3}He parameter Sets I and VI and the Rosen[29] neutron parameter Set I. The curves shown are the results of the calculations with the I-I optical parameter combination and bound state $r_0 = r_c = 1.15$ fm, $a_0 = 0.65$ fm. The calculated curves are individually normalized to the data. The fits to the angular distributions led to J^π assignments for all levels except for the state at 4.18 MeV. This state could be described equally well by either a 0^+ or a 2^+ calculation.

As might be expected the calculated relative magnitudes based on pure two-particle configurations did not agree with the observed relative strengths. This is a reflection of the large configuration asmixtures in the ^{60}Zn wave functions. The four-particle shell-model wave functions of Singh and Rustgi[46] (S) have been reported for the 0^+, 2^+, 4^+, and first excited 0^+ levels of ^{60}Zn assuming a doubly closed ^{56}Ci core. The components in these ^{60}Zn wave functions which overlap with an assumed ^{58}Ni core of $\nu(f_{7/2})^8 \pi(f_{7/2})^8 (p_{3/2})^2_{0^+}$ were extracted from the four-particle wave functions and were assumed to be the only components which could be reached in the transfer of a singlet diproton. Our analysis does not represent a rigorous test of the ^{60}Zn wave functions, but rather an attempt to reproduce the observed relative strengths with the wave functions and model available. Table VI shown a comparison of the experimental and
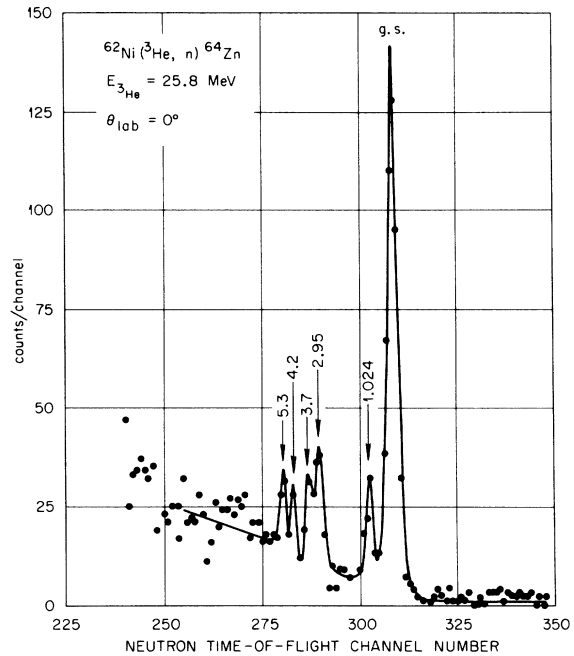

FIG. 11. Neutron time-of-flight spectrum for the ^{62}Ni(^{3}He,n)^{64}Zn reaction.

calculated magnitudes assuming the two-particle, closed-core overlap components S with the optical parameters which gave the best fits to the angular distributions I-S-I and VI-S-I. It may be argued from the consistency displayed in Table VI that:
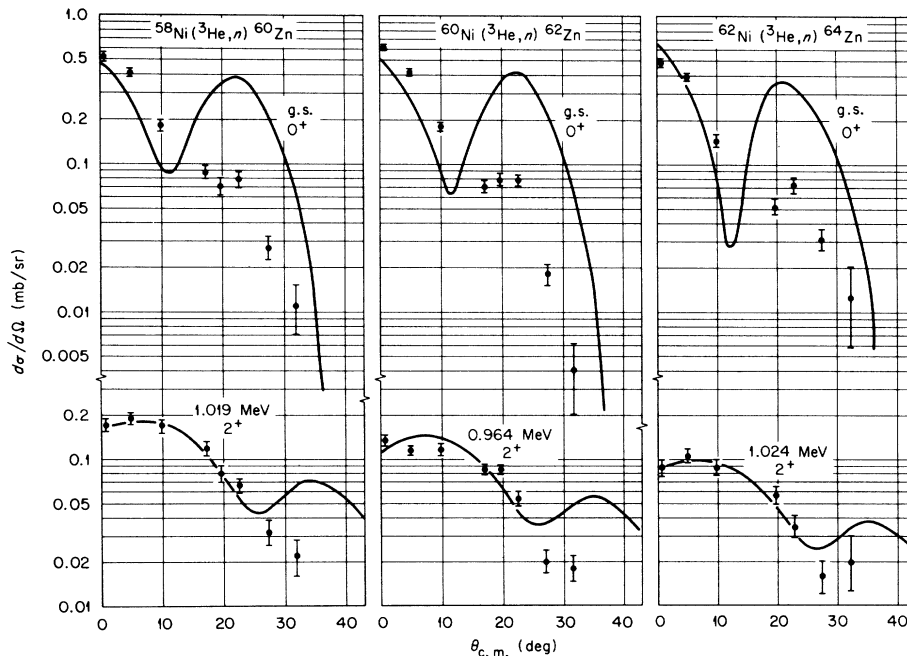

FIG. 12. Comparison of the angular distributions to the ground and first excited 2^+ states of ^{60}Zn, ^{62}Zn, and ^{64}Zn.

(1) Different optical-model parameters do not grossly affect the calculated cross sections; and (2) the experimental cross sections may be largely accounted for by assuming closed-core ground-state parentage.

Figures 10 and 11 show time-of-flight spectra for the ^{60}Ni(^{3}He, n)^{62}Zn and ^{62}Ni(^{3}He, n)^{64}Zn reactions, respectively. The cross sections for the ground-state transitions were approximately the same as for the 58–60 reactions. However, the cross sections to the excited states of the Zn isotopes decreased with increasing neutron number. Table III lists the energies of the neutron groups observed and, where available, the results of other experiments. Since it appeared that the higher excited transitions may have corresponded to more than one level, complete angular distributions were only obtained for the ground and first excited states of ^{62}Zn and ^{64}Zn. These are presented in Fig. 12. The groups of states near 3.5 and 5.5 MeV are excited consistently in the three Zn isotopes. This would seem to suggest similar structure for these states. Calculations were made with several choices of optical parameters. The calculated shapes of the angular distributions were nearly the same for the several different parameters sets. The curves shown are for the I-I optical potentials and the assumed two-particle configurations of $(p_{3/2})^2_{0^+}$ and $(p_{3/2})^2_{2^+}$. Both the calculated and experimental shapes of the angular distributions show a slight Q and mass dependence which presumably accounts for the slight differences in their shapes.

As in the (58–60) reaction, a comparison of the experimental relative magnitudes with the calculated relative magnitudes based on pure two-particle configurations produced very poor agreement. Shell-model calculations for ^{62}Zn and ^{64}Zn were not found in the literature. Since the coherent summation of two-particle components could not provide unique structure information, no attempt was made to determine the ^{62}Zn or the ^{64}Zn wave functions from comparison with the data. It is interesting to note, however, that although the ground-state transition strength remains nearly constant for the three isotopes, the strength to the excited states is significantly reduced with increasing neutron number. The ^{60}Zn nucleus has 30 protons and 30 neutrons. The neutrons added from one isotope to the next are entering the same shell orbitals populated in the reaction by the transferred protons. It seems then that the neutrons filling the same shells have a marked influence on the final-state wave functions, and the simple model of two-particle proton states in an effectively closed core is no longer applicable.

[1]D. G. Fleming, J. C. Hardy, and J. Cerny, Nucl. Phys. A162, 225 (1971).

[2]D. G. Fleming, M. Blann, H. W. Fulbright, and J. A. Robbins, Nucl. Phys. A157, 1 (1970).

[3]J. B. Ball, R. L. Auble, J. Rapaport, and T. A. Belote, Phys. Letters B37, 173 (1971).

[4]S. M. Smith, P. G. Roos, A. M. Bernstein, and C. Moazed, Nucl. Phys. A158, 497 (1970).

[5]J. Cerny and R. H. Pehl, Argonne National Laboratory Report No. ANL-6848, 1964 (unpublished), p. 208.

[6]R. Middleton and D. J. Pullen, Nucl. Phys. 51, 50 (1964).

[7]N. Glendenning, Phys. Rev. 137, B102 (1964).

[8]M. C. Lemaire, J. M. Loiseaux, M. C. Mermay, A. Papineau, and H. Faraggi, Phys. Rev. Letters 15, 900 (1970).

[9]H. W. Fulbright, W. P. Alford, O. M. Bilanuk, V. K. Deshpande, and J. W. Verba, Nucl. Phys. 70, 553 (1965).

[10]J. H. Manley, Phys. Rev. 130, 1475 (1963).

[11]J. H. Towle and G. J. Wall, Nucl. Phys. A118, 500 (1968).

[12]H. C. Bryant, J. G. Beery, E. R. Flynn, and W. T. Leland, Nucl. Phys. 53, 97 (1964).

[13]W. R. McMurray, P. Van Der Merwe, and J. J. Van Heerden, Nucl. Phys. A92, 401 (1967).

[14]R. G. Miller and R. W. Kavanagh, Nucl. Phys. A94, 261 (1967).

[15]D. D. Brill, A. D. Vonigai, V. S. Romanov, and A. R. Faiziev, Yadern. Fiz. 12, 253 (1970) [transl.: Soviet J. Nucl. Phys. 12, 138 (1971)].

[16]E. G. Adelberger and A. B. McDonald, Nucl. Phys. A145, 497 (1970).

[17]J. Singh, Nucl. Phys. A155, 443 (1970).

[18]M. J. Saltmarsh, C. D. Goodman, D. C. Hensley, and M. B. Greenfield, to be published.

[19]T. G. Miller, Nucl. Instr. Methods 63, 121 (1968).

[20]R. E. Textor and V. V. Verbinski, Oak Ridge National Laboratory Report No. ORNL-4160 (unpublished).

[21]R. H. Bassel, R. M. Drisko, and G. R. Satchler, Oak Ridge National Laboratory Report No. ORNL-3240 (unpublished).

[22]B. F. Baymen, Phys. Rev. Letters 25, 1768 (1970).

[23]E. Rost and P. D. Kunz, Nucl. Phys. A162, 376 (1971).

[24]R. Huby, M. T. Rafai, and G. R. Satchler, Nucl. Phys. 9, 94 (1958).

[25]W. Tobocman, Phys. Rev. C 1, 377 (1970).

[26]N. F. Mangelson, Univ. of California Report No. UCRL-17732 (unpublished).

[27]E. F. Gibson, B. W. Ridley, J. J. Kraushaar, and M. E. Rickey, Phys. Rev. 155, 1194 (1971).

[28]P. P. Urone, C. W. Put, H. H. Chang, and B.W. Ridley, Nucl. Phys. A163, 225 (1971).

[29]L. Rosen, J. C. Beery, A. S. Goldhaber, and E. H. Auerbach, Ann. Phys. (N.Y.) 34, 96 (1965).

[30]D. Wilmore and P. E. Hodgson, Nucl. Phys. 55, 676 (1964).

[31]F. Perey and B. Buck, Nucl. Phys. 54, 417 (1964).

[32]F. D. Becchetti and G.W. Greenlees, Phys. Rev. 182, 1197 (1968).

[33]R. M. Drisko and F. Rybicki, Phys. Rev. Letters 16, 275 (1965).

[34]S. Yoshida, Nucl. Phys. 33, 685 (1962).

[35]C. Maples, G. W. Goth, and J. Cerny, Lawrence Radiation Laboratory Report No. UCRL-16964 (unpublished).

[36]G. C. Ball and J. Cerny, Phys. Rev. 155, 1170 (1966).

[37]H. T. Fortune, T. J. Gray, W. Trost, and N. R. Fletcher, Phys. Rev. 179, 1033 (1969).

[38]B. J. Cole, R. Huby, and J. R. Mines, Phys. Letters 33B, 320 (1970).

[39]R. Huby, Phys. Letters 33B, 323 (1970).

[40]D. H. Youngblood, R. L. Kozub, R. A. Kenefick, and J. C. Hiebert, Phys. Rev. C 2, 477 (1970).

[41]J. C. Hardy, A. D. Bacher, G. R. Plattner, J. A. McDonald, and R. G. Sextro, Phys. Rev. Letters 25, 298 (1970).

[42]W. T. True, Phys. Rev. 130, 1530 (1963).

[43]J. B. McGrory, private communication.

[44]J. C. Hardy and R. I. Verrall, Phys. Letters 13, 148 (1964).

[45]J. Jaenecke, Z. Physik 160, 171 (1960).

[46]R. P. Singh and M. L. Rustgi, Phys. Rev. C 3, 1172 (1970).

FARADAY
CUP

BEAM
SWITCHING
MAGNET NO. 2

TARGET
POSITIONS

CLEARING
COLLIMATOR

DEFINING
COLLIMATOR

DETECTOR

45°

45° FLIGHT PATH

0°

0° FLIGHT PATH

BEAM
TRAJECTORIES
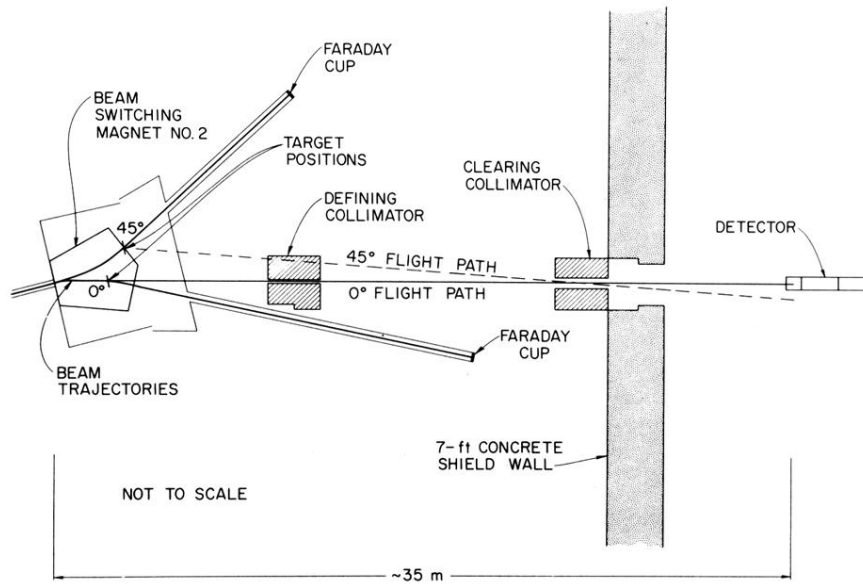
FARADAY
CUP

7- ft CONCRETE
SHIELD WALL

NOT TO SCALE

~35 m

FIG. 1. Schematic layout of the ORIC neutron time-of-flight line.